International Journal of Environmental Science and Technology (2025) 22:13983–13998
https://doi.org/10.1007/s13762-025-06555-6

ORIGINAL PAPER

Electrochemical deposition of N-doped ZnO film and its superior potential to inactivate microorganisms

M. K. Silva[1] · C. M. V. P. Ramos[1] · A. E. B. Lima[1] · R. M. P. Silva[1] · G. S. de Figueiredo[2] · R. A. Antunes[3] · W. Alves[4] · G. E. Luz. Jr[1] · R. S. Santos[1]

Received: 12 November 2024 / Revised: 21 March 2025 / Accepted: 29 April 2025 / Published online: 20 May 2025

Abstract

Nitrogen-doped ZnO (ZnO:N) is a semiconductor with enhanced photocatalytic properties, which makes it a promising material for antimicrobial applications. In this study, the photoelectrocatalytic inactivation of *Staphylococcus aureus*, *Escherichia coli* and *Candida albican* on ZnO:N films was investigated. The films were prepared by electrochemical deposition with different doping concentrations (20, 40, 60 cm^3 min^{-1}). X-ray diffraction patterns showed that pure ZnO and ZnO:N films displayed a crystalline wurtzite structure. Scanning electron micrograph revealed a hexagonal nanorod morphology for samples. The substitutional doping that occurred in ZnO favored the formation of oxygen vacancies, as shown by X-ray photoelectron spectroscopy measurements. The nitrogen doping caused a decrease in the values of the band gap energy (E_{bg}) from 3.17 to 3.12 eV. Photoelectrochemical studies showed higher photocurrent density for ZnO:N compared to ZnO films, reaching 60 µA cm^{-2} at 0.70 V (vs. Ag/AgCl). The chronopotentiometry curves showed that all films present n-type semiconductor behavior and flat band potentials suitable for generating reactive oxygen species capable of inactivating microorganisms. Under irradiation, all ZnO:N films inhibited *S. aureus*. Also, ZnO:N-40 film showed complete inhibitory effects on *E. coli* and *C. albicans.* These results highlight the potential of nitrogen-doped ZnO films for antimicrobial applications.

Keywords N-doped ZnO films · Electrodeposition · Antibacterial activity · Antifungal · Wastewater treatment

Introduction

The presence of pathogenic microorganisms such as bacteria and fungi on material surfaces poses a challenge from both economic and public health perspectives. Recently, the SARS-CoV-2 pandemic has spurred interest in materials capable of keeping sanitized surfaces and environments (Catalano et al. 2016). Surfaces with high human contact frequently offer many opportunities for microbial transmission. Although conventional cleaning products have immediate disinfectant capacity, many cleaning products based on volatile solvents tend to lose their effectiveness quickly (Ejerhed et al. 2020). Therefore, efforts are directed toward strengthening prevention through the development of antibacterial coatings with natural and synthetic organic compounds formed by more stable inorganic substances (Costa et al. 2019). Recently, Birkett et al. (Birkett et al. 2022) discussed that these coatings, when applied to high-contact surfaces in healthcare settings such as hospitals, are effective in reducing infections.

Recent advances in materials science have shown that research on semiconductors has the potential to inhibit bacteria, viruses, and other pathogens. Among the semiconductors exhibiting such activity, compounds containing silver (Khare et al. 2019; Camargo et al. 2023), gold (Ahmad et al. 2013; Balestri et al. 2023), titanium (Escárcega-González et al. 2018; Tang et al. 2023), copper (Amiri et al. 2017),

Editorial responsibility: Samareh Mirkia.

✉ A. E. B. Lima
alinebrandao08@gmail.com

1 PPGQ-GrEEnTec-Chemistry Department, State University of Piauí-UESPI, 2231 João Cabral Street, P.O. Box 381, Teresina, PI 64002-150, Brazil

2 Department of Parasitology and Microbiology, Federal University of Piauí-UFPI, Campus Ministro Petrônio Portella, Ininga, Teresina, PI 64049-550, Brazil

3 Center for Engineering, Modeling and Applied Social Sciences, Federal University of ABC/UFABC, Bangu, Santo André, SP 09210-580, Brazil

4 IPEN/CNEN, Institute for Energy and Nuclear Research, University City, São Paulo, SP 05508-000, Brazil

and zinc (Yurtsever et al. 2024; Antonette and Shanthi 2023) are notable. Zinc oxide (ZnO), for instance, is an n-type semiconductor with a band gap (E_{bg}) of 3.37 eV (Chen et al. 2017). It can exist in two structural types: cubic or hexagonal (wurtzite). The hexagonal phase is thermodynamically more stable at room temperature (Hessien 2022) and exhibits important properties, including low cost, high photocatalytic activity, and low toxicity (Kabir et al. 2020). Due to its good thermal stability, high antimicrobial activity, and excellent biocompatibility, ZnO is a potential threat to environmental microorganisms, being a promising and effective antibacterial agent against both Gram-negative and Gram-positive bacteria (Applerot et al. 2009; Pasquet et al. 2014). This metallic oxide is commonly found in pharmaceutical formulations, such as in the composition of ointments for diaper rash in children and medications for burn treatment. In this context, our research group recently investigated a formulation having ZnO, silver nanoparticles (AgNP), and wild plum extract, which was successfully applied in the treatment of burn-induced wounds (Carneiro et al. 2022).

Studies have shown that various ZnO-containing materials exhibited activity against *Staphylococcus aureus (S. aureus)* (Biron et al. 2021), *Escherichia coli* (Kumar et al. 2021), *Candida albicans* (Miri et al. 2019), and other strains. *S. aureus* is a Gram-positive bacterium with broad distribution, posing significant risks to the body and capable of causing a range of infections. Known as the main cause of hospital infections, it poses a significant threat transmitted by contaminated equipment or environmental sources (Khatoon et al. 2023; Zhang et al. 2023a). Escherichia coli, a Gram-negative bacterium, is a leading cause of diarrheal diseases and the most commonly used indicator of fecal contamination in drinking water. Widely recognized as a pathogen, it is associated with both community-acquired and hospital infections, causing a variety of intestinal and extraintestinal diseases (Basu et al. 2021). The fungus *C. albicans* is responsible for hospital infections, causing significant morbidity and mortality. It proves the ability to colonize various tissues, such as the skin, mucous surfaces, oral cavity, vagina, and gastrointestinal tract, causing recurrent mucosal infections and contagious infections with potential life-threatening risks and a high mortality rate (Dananjaya et al. 2018; Sachivkina et al. 2021).

Doping has been studied as a method to improve the properties of ZnO thin films. Thus, selectively added dopants to ZnO offer a significant route to control and enhance its optical, electrical, structural, thermal, and biological effects (Mu et al. 2011; Gu et al. 2011). This method involves incorporating metals and non-metals into the crystal structure. In comparison, non-metallic doping proves more efficient than metallic dopants due to its good stability and better electron/hole separation. In this context, nitrogen (N) has been considered a suitable impurity due to its similarities in electronegativities and ionic radio with N and O (Qi et al. 2017). For instance, Gupta et al. (2016) describe N-doped ZnO through a combustion synthesis followed by a hydrothermal method for antibacterial applications, resulting in enhanced photocatalytic activity against *E. coli*.

Thin films of doped and non-doped ZnO can be obtained by various methods, including sol–gel (Sinornate et al. 2022), hydrothermal (Zhang et al. 2023b), radiofrequency magnetron sputtering (Hopoğlu et al. 2021), spray pyrolysis (Ardekani et al. 2018), and solvothermal (Wu et al. 2014). In an earlier study (Reis et al. 2020), our research group prepared ZnO:N films by an electrochemical method, which showed superior photostability and photocatalytic activity for the oxidation of Rhodamine B in aqueous solution. Thus, this research aims to investigate the production of ZnO and ZnO:N films, based on a method previously studied by our

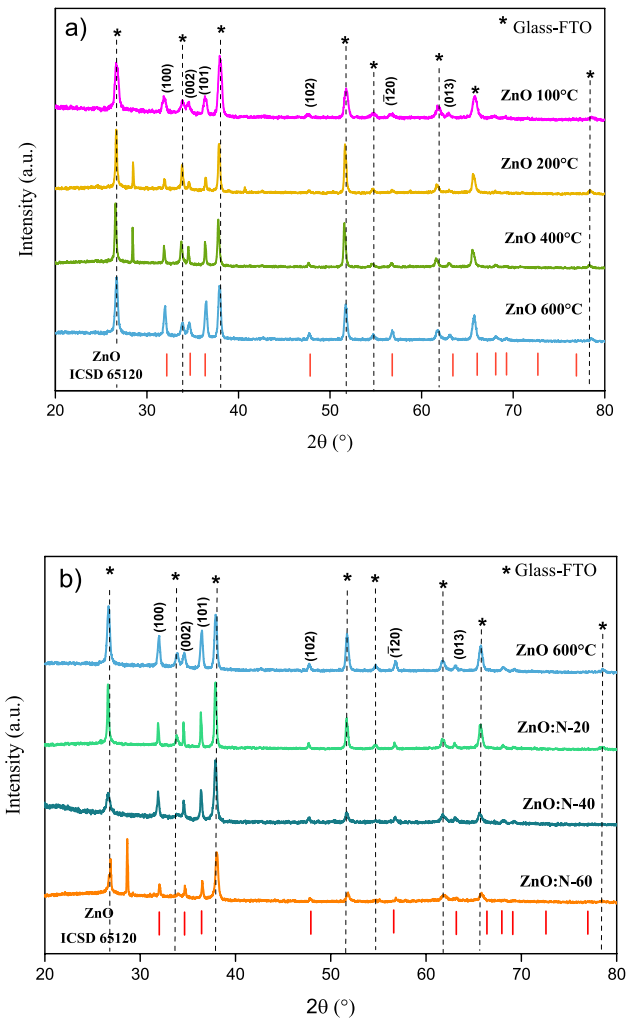

Fig. 1 XRD patterns of **a** ZnO films calcined at 100, 200, 400, and 600 °C; **b** ZnO:N films (20, 40, and 60 cm^3 min^{-1}) calcined at 600 °C. Vertical lines (|) indicate the positions of hexagonal ZnO planes

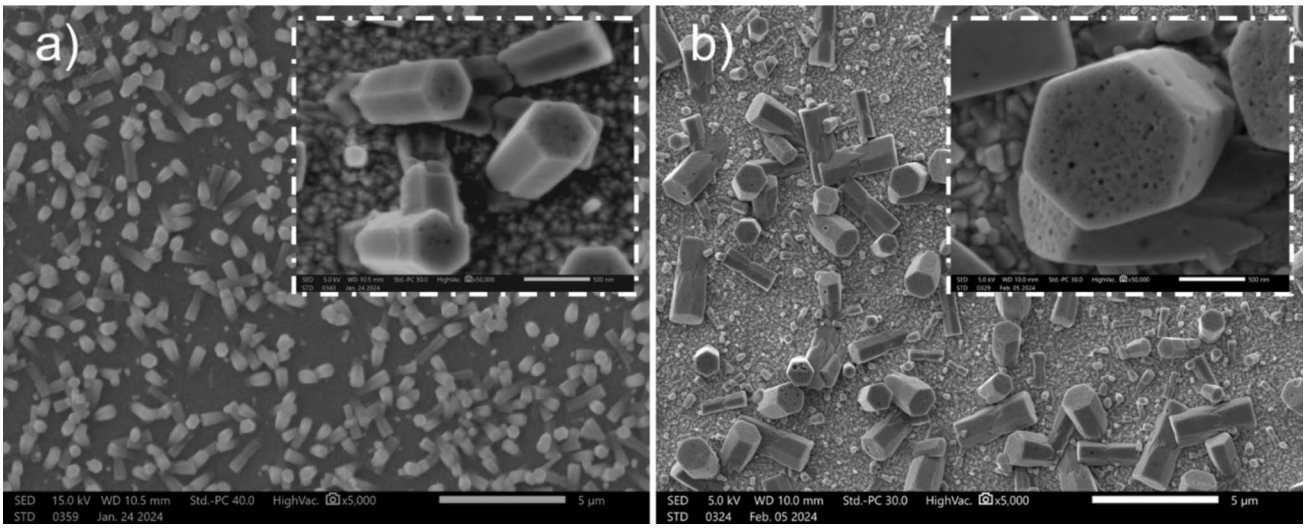

Fig. 2 FE-SEM images of **a** ZnO films heat treated at 600 °C and **b** ZnO:N-40. The inset shows high-magnification (50 k) of the samples

research group, and their application as promising materials for the inactivation of a Gram-positive bacterium (*S. aureus*), a Gram-negative bacterium (*E. coli*), and a yeast species (*C. albicans*), a unicellular fungus. The inactivation was evaluated both in the absence of light (dark conditions) and under irradiation with a polychromatic light source. To our knowledge, this is the first study on the biocidal activity of nitrogen doped ZnO electrodes (ZnO:N) with the aim of inactivating microorganisms.

Materials and methods

Electrochemical synthesis of ZnO and ZnO:N films

The electrodeposition of ZnO and ZnO:N films was performed based on a methodology previously investigated by our research group (Reis et al. 2020). Thus, the electrodeposition of the thin films was performed in a three-electrode electrochemical cell. Zinc oxide (ZnO) and nitrogen-doped zinc oxide (ZnO:N) were deposited onto the working electrode, which consisted of a fluorine-doped tin oxide (FTO) conductive substrate. Ag/AgCl (sat. KCl) electrodes and platinum wire were used as the reference electrode and counter electrode, respectively.

Initially, the FTO substrates were cleaned through three consecutive steps in an ultrasonic bath: first with water and neutral detergent, followed by deionized water, and finally with isopropyl alcohol. Each cleaning step lasted 15 min. After the cleaning process, the substrates were air-dried at room temperature. Then, the electrodeposition of the ZnO film was carried out at a constant potential of − 0.9 V for 30 min, using an aqueous solution containing 5 mmol L^{-1} of of zinc acetate dihydrate ($Zn(CH_3COO)_2{\cdot}2H_2O$; 99%) as the precursor and 0.1 mol L^{-1} KCl as the supporting electrolyte. The system was maintained at 75 °C, continuously stirred, and bubbled with air at a flow rate of 100 cm^3 min^{-1} during the deposition process. After deposition, the thin films were air-dried at room temperature and subjected to thermal treatment at various temperatures (100–600 °C) in a muffle furnace (Reis et al. 2020).

The deposition of ZnO:N films was performed under conditions similar to those used for ZnO films, with an additional step of nitrogen gas (N_2) bubbling at varying flow rates of 20, 40, and 60 cm^3 min^{-1}, alongside air bubbling. To maintain a total gas flow rate of 100 mL min^{-1} during the synthesis, synthetic air and N_2 flow rates were adjusted accordingly. For instance, when the N_2 flow rate was set to 40 mL min^{-1}, the synthetic air flow rate was reduced to 60 mL min^{-1}. After deposition, the ZnO:N films were thermally treated at 600 °C for 1 h in a muffle furnace, using a heating rate of 10 °C min^{-1}. The samples were designated ZnO:N-20, ZnO:N-40, and ZnO:N-60, corresponding to the respective N_2 flow rates used during their preparation.

Films characterizations

The X-ray Diffraction (XRD) patterns of the films were obtained using a D8-Advance ECO X-ray diffractometer (Bruker), employing Cu-Kα radiation (λ = 0.154 nm) at 40 kV and 25 mA, with an incident diffraction angle 2θ ranging from 20° to 90° and a scanning speed of 0.02°. The diffraction patterns were compared with data from the *Inorganic Crystal Structure Database* (ICSD). The surface morphology was obtained by field emission scanning electron microscopy (FEG–SEM) using a JSM-IT700HR. X-ray

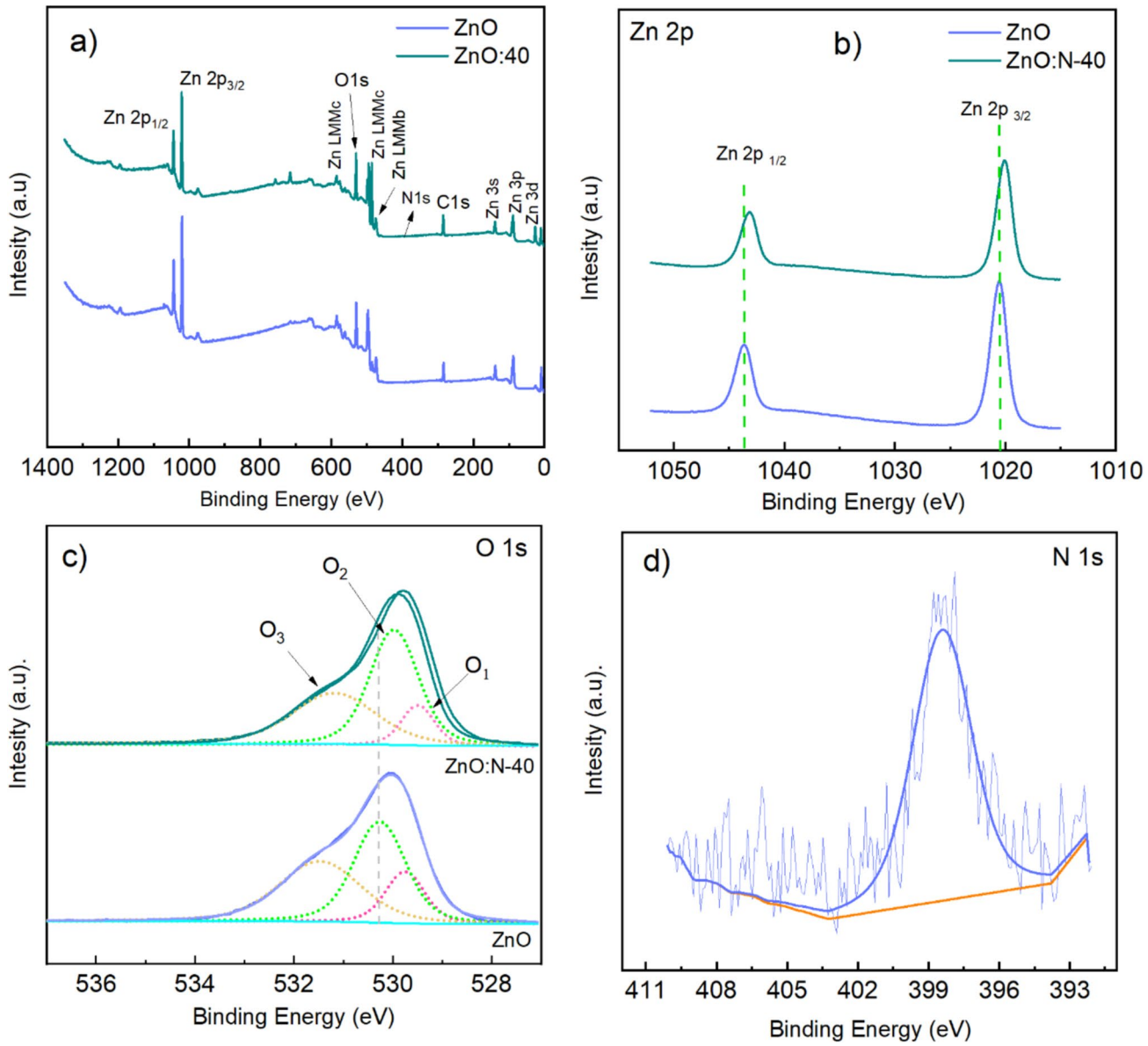

Fig. 3 XPS spectra of **a** Survey spectra ZnO and ZnO:N-40 films and high resolution XPS spectrum **b** Zn 2p, **c** O 1 s, and **d** N 1 s

Excited Photoelectron Spectroscopy (XPS), employing the K-alpha + model provided by Thermo Fisher Scientific and an Al-kα X-ray source, was employed to investigate the surface elemental composition and characterize the chemical binding states in the samples. The analysis chamber was kept at a pressure of approximately 10^{-7} Pa, with a spot size measuring 400 µm. Pass energies for survey and high-resolution spectra were set to 50 eV and 20 eV, respectively. The thin films underwent optical and electrochemical characterization. Optical properties were analyzed using UV–Vis spectroscopy with a Shimadzu UV-2600 spectrophotometer.

Photoelectrochemical measurements

Photoelectrochemical properties were analyzed using a potentiostat/galvanostat (Autolab PGSTAT 320-N Metrohm) with NOVA 1.7 software. A photoelectrochemical cell was used, employing a three-electrode configuration and an aqueous solution of 0.1 mol L^{-1} Na_2SO_4 as a supporting electrolyte. The ZnO and ZnO:N films served as the working electrodes. A Pt wire was employed as the counter electrode, while Ag/AgCl was used as the reference electrode both in the absence of light (dark) and under irradiation using a polychromatic light source, using a metal vapor lamp (Osram HQI-TS NDL) with a nominal power of 150 W. The photoelectrochemical studies were carried out by

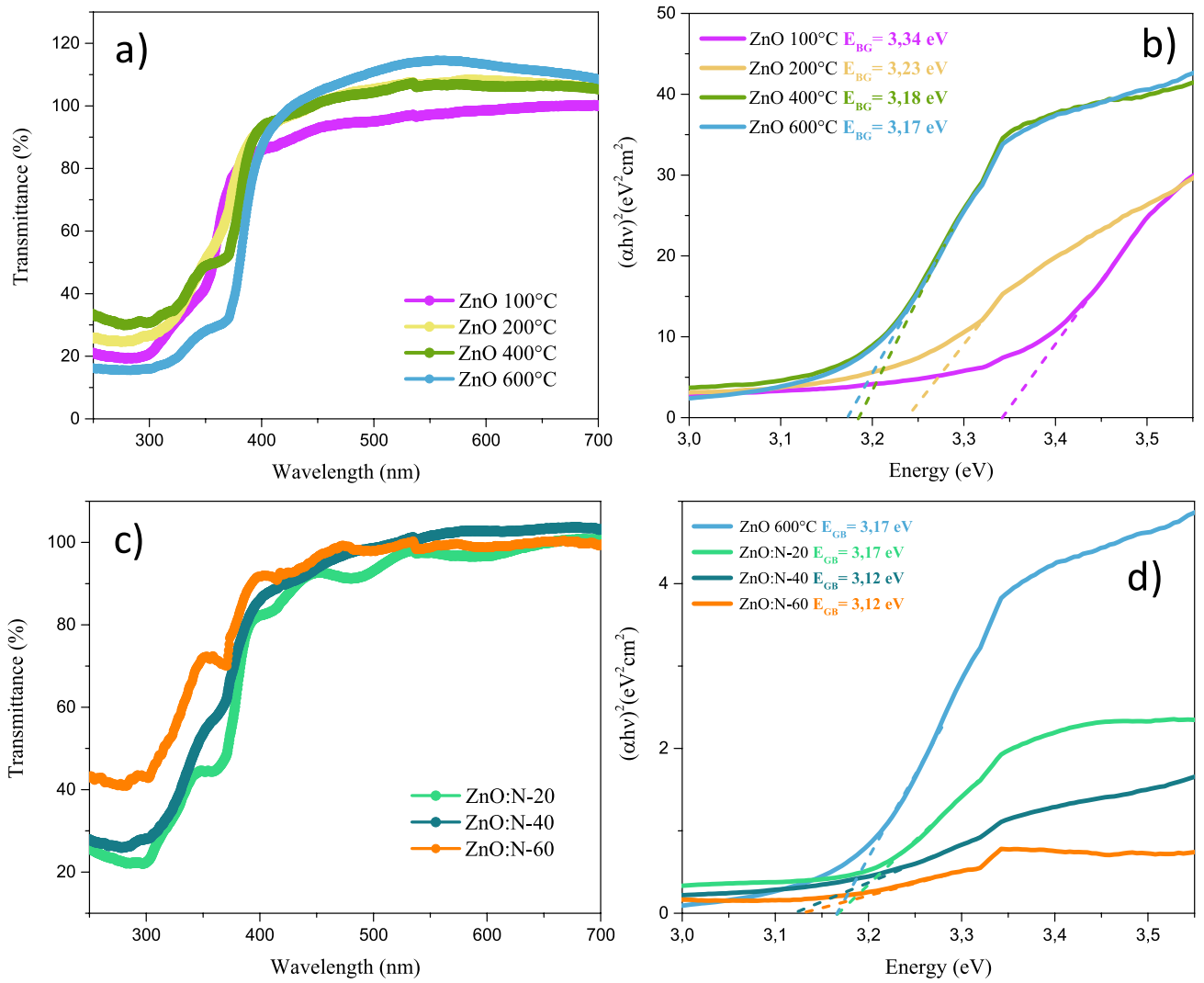

Fig. 4 **a** UV–vis transmittance curves for thin ZnO films annealed at 100 °C, 200 °C, 400 °C, and 600 °C, **b** estimation of E_{bg} using the TAUC method for ZnO, **c** transmittance curves for films of ZnO doped with 20, 40 and 60 cm^3 min^{-1}, **d** estimation of E_{bg} for doped ZnO

adjusting the irradiation power to 100 mW cm^{-2} using a Newport Power Meter, model 843-R. The spectrum distribution pattern of polychromatic light is shown in Fig. 1S of the Supporting Information (SI).

The photocurrent density was measured using cyclic voltammetry (CV) in the dark and under polychromatic irradiation. The flat band potentials (E_{fb}) of the oxides were estimated by the Burtler–Gärtner method, using light–dark linear sweep voltammetry (LSV) data collected in the anodic potential range of − 0.1 to 1.0 V, with a scan rate of 1.0 mV/s and manual chopper operation at a frequency of 0.1 Hz. The transient photocurrent of the films was measured using chronoamperometry polarized at a potential of 0.7 V. The potentials were converted to the Reversible Hydrogen Electrode (RHE) scale and subsequently to electron volts (eV) using Eqs. 1 and 2, respectively (Pitombeira et al. 2023).

$$E\ (\text{vs. RHE}) = E\ (\text{vs. Ag/AgCl}) + 0.0591\ \text{V x pH} + 0.199\ \text{V} \quad (1)$$

$$E(\text{eV}) = [-4.5\ \text{eV} - eE\ (\text{RHE})] \quad (2)$$

Microorganisms inactivating tests

For the photoelectrocatalytic inactivation tests of ZnO and ZnO:N, three standard microbial strains were used, namely: *S. aureus*—ATCC 25923 (a Gram-positive bacterium), *E. coli* ATCC 25922 (a Gram-negative bacterium), and the fungus *C. albicans* ATCC 10231 (a yeast species, unicellular fungus).

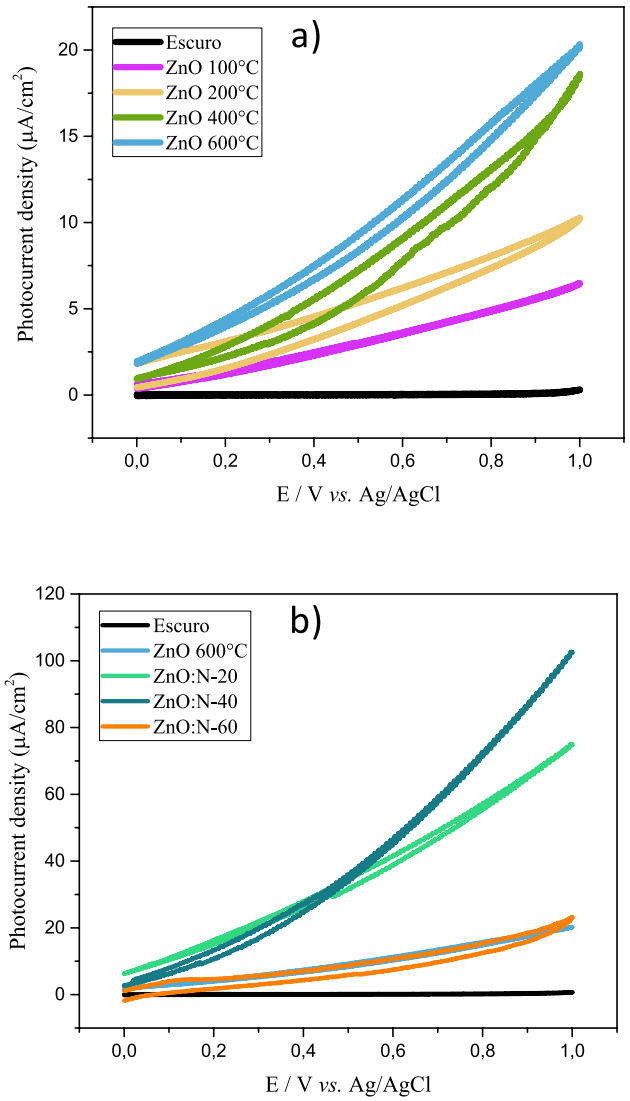

Fig. 5 Cyclic voltammograms with dark and irradiated curves collected at a 10 mV s^{-1} scan rate, **a** ZnO electrodes at different temperatures (100, 200, 400 °C, and 600 °C), and **b** ZnO:N electrodes with flow rates of 20, 40, 60 cm^3 min^{-1} annealed at 600 °C

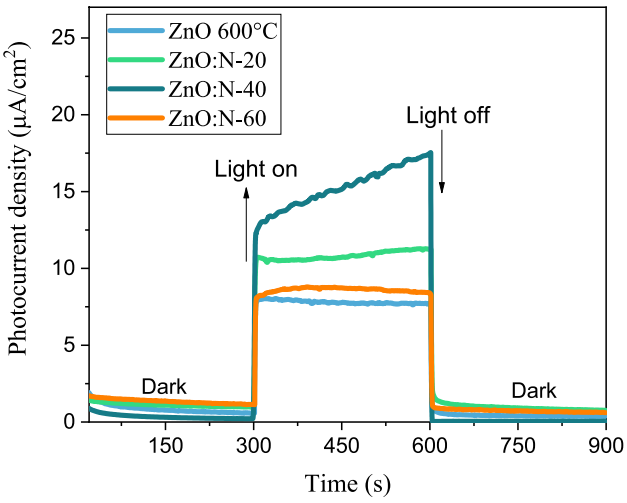

Fig. 6 Chronoamperometric curves with light interruption every 300 s, under bias potential of 0.7 V (vs. Ag/AgCl) for ZnO and N-deoped ZnO:N films

The microbial species were kept in KASVI brand culture media, with Brain Heart Infusion (BHI) agar for the bacterial species and Sabouraud Agar for the yeast species. All species were incubated in a Biological Oxygen Demand (BOD) incubator at 37 °C for a period of 24 h for bacteria and 48 h for yeast. Microbial cell suspensions were prepared in 0.8% NaCl, containing 10^8 cells/mL, corresponding to a 0.5 McFarland scale. The inactivation tests were carried out in a photoelectrochemical cell containing 13.5 mL of Na_2SO_4 and 500 µL of microbial suspensions. The photoelectrocatalytic tests were performed using a potentiostat/galvanostat in chronoamperometry mode with a potential of 0.7 V, both in the absence of light (dark) and under irradiation with a polychromatic light source, using a lamp with a nominal power of 150 W to irradiate the samples. Similar to what was described for the photoelectrochemical studies, presented in Sect. 2.3, the light irradiance used in the microorganism inactivation test was adjusted to 100 mW cm^{-2}. Following irradiation under bias conditions, 100 µL of samples were collected at 10, 20, and 30-min intervals. These aliquots were plated on Petri dishes containing BHI media (for bacteria) and Sabouraud media (for yeast) and then incubated in a BOD incubator for 24 and 48 h for bacteria and fungi, respectively. After this incubation period, colony counts were conducted on the colonies grown on these plates. Plates containing culture media and a suspension of microorganisms in Na_2SO_4, without ZnO, were used as a control group.

Results and discussion

Structural characterization

XRD measurements were carried out on the films subjected to heat treatment at 100, 200, 400, and 600 °C, as well as on ZnO prepared in the presence of N_2 with flow rates of 20, 40, and 60 cm^3 min^{-1}, and calcined at 600 °C. These results can be seen in Fig. 1.

Based on the analysis of Fig. 1, it is noted that all synthesized materials exhibit XRD signals correctly indexed to the hexagonal wurtzite structure of ZnO. The positions of the XRD signals in the diffractograms align with the results recorded in the *Inorganic Crystal Structure Database* (ICSD) under N°. 65120 (Albertsson et al. 1989), where the diffraction peaks coincide with the reflection planes

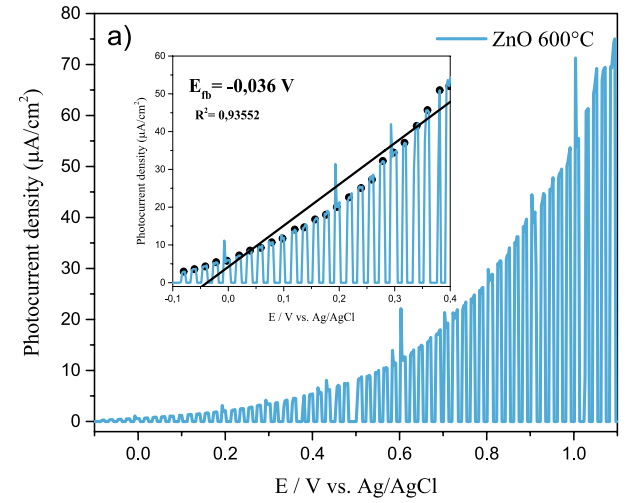

Fig. 7 Linear sweep voltammograms (LSV) of **a** ZnO, **b** ZnO:N-40 at 600 °C, under sequential chopper illumination of 10 s with an anodic potential range from − 0.1 to 1.0 V (vs. Ag/AgCl) at a scan rate of 1.0 mV s^{-1}. Inset: J^2 vs. V curves by the Butler-Gärtner model

(100), (002), (101), (102), (120), and (013) for hexagonal-structured ZnO (Wurtzite). For both films (doped and non-doped), signals were recorded at 2θ equal to 26.8°, 33.8°, 37.9°, 51.5°, 54.6°, 61.7°, 65.7°, and 78.4°, which can be attributed to SnO_2 composing the conductive layer (FTO). These signals were observed in all samples and are highlighted by a dashed vertical line and an asterisk (*). The ZnO:N films prepared with different nitrogen flow rates (20, 40 and 60 cm3 min^{-1}) showed a shift in diffraction signals to higher values of 2 theta, which may be attributed to the introduction of N atoms into the oxide crystal lattice (Mondal et al. 2023).

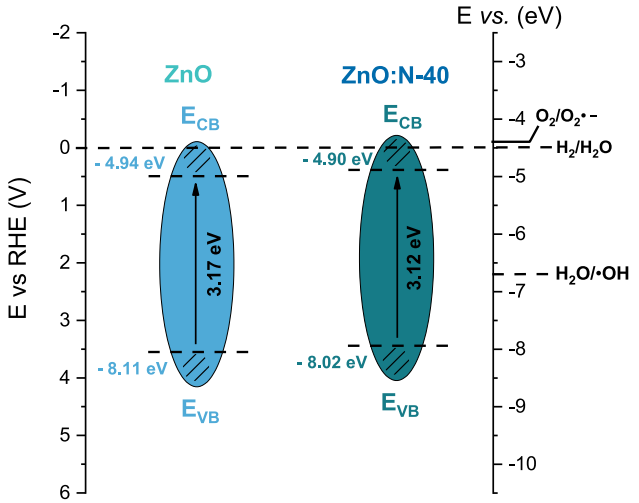

Fig. 8 Position of the valence band (VB) and conduction band (CB) edges for ZnO and ZnO:N-40 thin films

Morphological characterization

Based on superior photoelectrochemical response, the pure ZnO and ZnO:N-40 films heat treated at 600 °C have been singled out for further investigation. FEG-SEM analysis investigates the surface morphology of the films. Figure 2a reveals that pure ZnO film consisted of hexagonal nanorods with a length of around 0.62 µm. In the case of ZnO:N-40 (Fig. 2b), although the shape remains similar, there is a decrease in the average length of nanorods (0.41 µm ±0.16) because of N-doping (Mondal et al. 2023). The particles size reduction can enhance the surface area and improve its photocatalytic performance (Al-Gariaa et al. 2023). The high magnification given as insert Fig. 2b highlights the hexagonal nanorod morphology.

XPS analysis

X-ray photoelectron spectroscopy (XPS) was performed to obtain the surface elemental composition and identify the chemical binding states of the ZnO and ZnO:N-40 films. The survey spectra of the films reveal peaks corresponding to the presence of Zn, O, C, and N (Fig. 3a). The C 1 s peak at around 284.6 eV may be attributed to the adsorption process present in ambient conditions. The high-resolution Zn 2p spectrum exhibited binding energies of 1043.7 eV and 1020.5 eV, corresponding to Zn $2p^{1/2}$ and Zn $2p^{3/2}$, respectively (Fig. 3b). The shift of these peaks toward lower binding energy in ZnO:N-40 can be attributed to the presence of N atoms that substituted for O and bonded to Zn atoms (Khalid et al. 2022; Li et al. 2015).

The O 1 s spectra (Fig. 3c) are deconvoluted into three peaks found at 529.7 eV (O_1), 530.3 eV (O_2), and 532.0

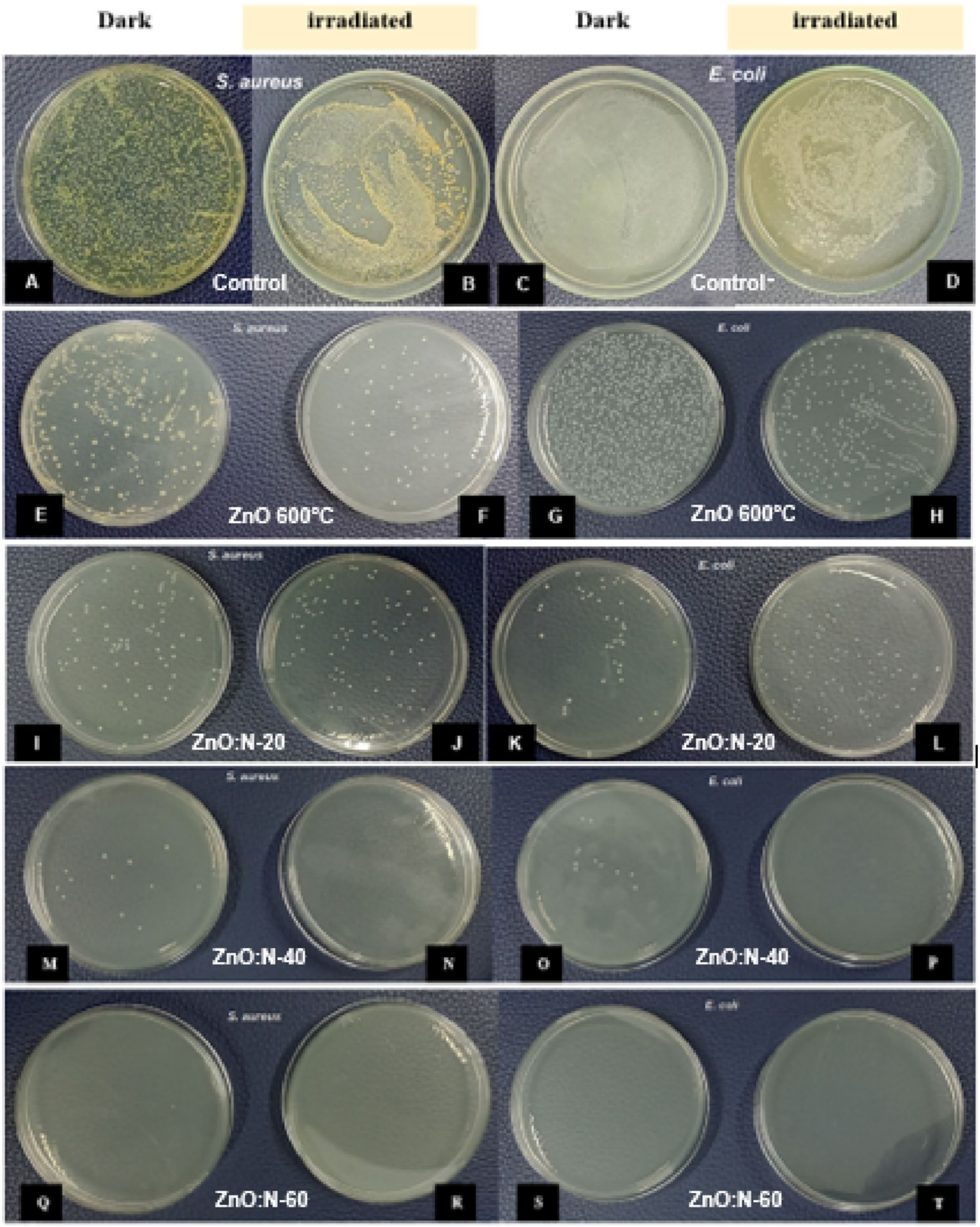
Dark
irradiated
Dark
irradiated
S. aureus
E. coli
A
Control
B
C
Control-
D
E
ZnO 600°C
F
G
ZnO 600°C
H
I
ZnO:N-20
J
K
ZnO:N-20
L
M
ZnO:N-40
N
O
ZnO:N-40
P
Q
ZnO:N-60
R
S
ZnO:N-60
T

◂**Fig. 9** Number of colonies grown after seeding in: **A**, **B** control of *S. aureus* growth in the dark and irradiated, **C**, **D** control of *E. coli* growth in the dark and irradiated, **E**, **F** colonies of *S. aureus* with ZnO 600 °C in the dark and irradiated, **G**, **H** colonies of *E. coli* with ZnO 600 °C in the dark and irradiated, **I**, **J** colonies of *S. aureus* with ZnO:N-20 in the dark and irradiated, **K**, **L** colonies of *E. coli* with ZnO:N-20 in the dark and irradiated, **M**, **N** colonies of *S. aureus* with ZnO:N-40 in the dark and irradiated, **O**, **P** colonies of *E. coli* with ZnO:N-40 in the dark and irradiated, **Q**, **R** colonies of *S. aureus* with ZnO:N-60 in the dark and irradiated, **S**, **T** colonies of *E. coli* with ZnO:N-60 in the dark and irradiated, respectively

eV (O_3), which correspond to the Zn–O in the wurtzite structure, oxygen vacancies (V_o), and chemisorbs oxygen on the surface, respectively. The lower binding energy for N-doped ZnO indicates increased defects through the substitutional doping process (Reis et al. 2020). Furthermore, the deconvolved O 1 s spectra revealed a higher concentration of oxygen vacancies. The O_2/O_1 ratio for ZnO was 2.56, and that for ZnO:N-40 was 4.16. The higher O_2/O_1 ratio for the ZnO:N-40 film, compared to ZnO, shows that adding N generates oxygen vacancies (Li et al. 2015). The substitutional doping is confirmed by deconvolution of the N 1 s peak at 398.4 eV (Fig. 3d) (Perkins et al. 2005). The increase in oxygen vacancies can enhance the photocatalytic activity of ZnO:N-40 film.

Estimative of the band gap energy for the ZnO and ZnO:N films

UV–Vis spectroscopy was employed to investigate the optical behavior of the films prepared in different conditions of temperature and nitrogen flux. Figure 4a, c illustrate that both ZnO and ZnO:N films maintain high transmittance at wavelengths above 450 nm. However, an abrupt absorption is seen close to 400 nm. For ZnO samples, heat treatment shifted the light absorption region to longer wavelengths, suggesting that the material became more crystalline. Thus, ZnO:N films, prepared in different conditions of nitrogen flux were calcined at 600 °C.

Based on the results obtained from the transmittance spectra of samples, it is possible to estimate the value of the "optical band gap energy" (optical E_{bg}) of this material, calculated using the Tauc method, assuming an indirect optical transition, according to Eq. 3: (Barbosa et al. 2023)

$$(\alpha h\nu)^n = C\,(h\nu - E_{bg}) \tag{3}$$

where α is the optical absorption coefficient of the film, $h\nu$ is the energy of the incident photon, C is a proportionality constant, E_{bg} is the band gap interval between the bottom of the conduction band and the top of the valence band, and n is equal to 1/2 for an indirect transition. The E_{bg} was calculated by extrapolating the linear part of the graph to where $(\alpha h\nu)^{1/2}$ equals zero, as shown in Fig. 4b, d.

The band gap values for the pure ZnO films annealed at 100, 200, 400, and 600 °C (Fig. 4a, b) were 3.34, 3.23, 3.17, and 3.17 eV, respectively. These values agree with those found in the literature (Tiron et al. 2017). For the films prepared with N_2 at flow rates of 20, 40, and 60 $cm^3\ min^{-1}$ (Fig. 4d), the E_{bg} value was 3.17, 3.12, and 3.12 eV, respectively. The E_{bg} data show that nitrogen doping did not result in a substantial change in the band gap value.

Photoelectrochemical properties

The photoelectrochemical properties of ZnO films annealed at the different temperatures investigated, as well as ZnO:N films at 600 °C (20, 40, and 60 $cm^3\ min^{-1}$), were analyzed in the dark and under polychromatic irradiation. The studies were conducted in a three-electrode electrochemical cell using a 0.1 mol L^{-1} aqueous solution of Na_2SO_4 as the supporting electrolyte. Figure 5 shows the photocurrent densities for the electrodes using cyclic voltammetry under dark and polychromatic irradiation conditions (10 mVs^{-1}).

The cyclic voltammetry curves for the electrodes under dark conditions showed nearly negligible capacitive current. To investigate the influence of annealing temperature on the photoelectrochemical response of ZnO films, the ZnO electrodes were annealed at 300, 400, 500 and 600 °C, as shown in Fig. 5a. Under polychromatic irradiation, it was seen that the increase in annealing temperature favored an increase in the photocurrent density of the films. The ZnO electrodes annealed at 300, 400, and 500 °C showed low photocurrent values. The ZnO electrode at 600 °C showed a better photocurrent density of approximately 12 μA cm^{-2} at 0.7 V (vs. Ag/AgCl). Consequently, all subsequent photoelectrochemical studies were performed by the N-doped electrodes annealing at 600 °C.

Figure 5b displays the voltammograms for the ZnO films prepared in N_2 with flow rates of 20, 40, and 60 $cm^3\ min^{-1}$, in comparison to undoped ZnO. The films with flow rates of 20, 40 and 60 $cm^3\ min^{-1}$ showed photocurrent values of approximately 47, 60, and 38 μA cm^{-2} at 0,7 V (vs. Ag/AgCl), respectively. The increase in N_2 flow from 20 to 40 $cm^3\ min^{-1}$ resulted in a significant enhancement in photocurrent. The ZnO:N electrode with a flow rate of 40 $cm^3\ min^{-1}$ showed superior photocurrent density, indicating that films prepared in the presence of N_2 allowed for greater electron mobility and improved electron transfer efficiency. This suggests a potential substitution of O atoms by N atoms in the ZnO structure or the presence of N atoms in the interstitial sites (Reis et al. 2020).

Table 1 Bactericidal activity of ZnO and ZnO:N films 20, 40, 60 cm^3 min^{-1}, under dark and irradiated conditions against *S. aureus* and *E. coli*

Sample (condition)	Number of microorganism colonies per inactivation time (min)					
	S. aureus			*E. coli*		
	10 min	20 min	30 min	10 min	20 min	30 min
Only action of light	*	*	*	*	*	*
ZnO (dark)	202	131	178	*	*	*
ZnO (irradiated)	26	46	50	314	362	252
ZnO:N-20 (dark)	50	27	24	152	100	100
ZnO:N-20 (irradiated)	74	30	34	70	60	40
ZnO:N-40 (dark)	15	11	11	7	6	10
ZnO:N-40 (irradiated)	–	–	–	–	–	–
ZnO:N-60 (dark)	4	2	–	–	–	–
ZnO:N-60 (irradiated)	–	–	–	–	–	–

Electrochemical measurements of films provide important information on charge transfer properties, especially for the application of films as photoelectrodes. In Fig. S2, chronopotentiometry curves recorded at dark–light intervals are presented in a 0.1 mol L^{-1} Na_2SO_4 solution under Open Circuit Potential (OCP) conditions for 300 s. Initially, the electrochemical system is in the dark, with a charge equilibrium at the electrolyte–electrode interface. After irradiation, there is an electron transition from the valence band (VB) to the conduction band (CB) of the material. Considering the band theory and charge transfer at the electrolyte–electrode interface, when irradiation stops, electrons return from CB to VB, overcoming the material defects. Thus, considering the experiment chronopotentiometry time (100 s), only ZnO:N-40 film returned to a steady-state of photopotential after radiation ceased. The negative photopotential values ($\Delta E = E_{Light\ on} - E_{\ light\ off} < 0$) presented in Table S1 are indicative of an n-type semiconductor behavior. This result suggests that ZnO doped with a higher amount of nitrogen has a greater number of defects (traps), generating localized levels between the VB and CB, and preventing the rapid electron transfer. Furthermore, the most suitable dopant concentration was achieved with a nitrogen gas flow of 40 mL min^{-1} for film preparation via the electrochemical route.

The photocurrent intensity of ZnO and N-doped ZnO electrodes can be related to a longer recombination lifetime of electron–hole pairs (e^-_{CB}/h^+_{VB}), formed after irradiation of the semiconductor. Based on the chronoamperometric curves recorded under dark interruption conditions every 300 s, presented in Fig. 6, it is possible to evaluate the effectiveness of the charge separation process in each film. Immediately after irradiation, a photocurrent signal is formed, which can be associated with a charge separation process, with the injection of electrons into the CB of the semiconductor. Photocurrent means that electrons from the semiconductor are conducted towards the counter-electrode, while holes in the VB react with species present in the electrolyte. Our previous studies have shown that even under irradiation, a gradual reduction in photocurrent over time indicates that there is an equilibrium in the concentrations of electrons in the CB and holes in the VB, reaching a steady-state current (Resende et al. 2021). Charge recombination can occur with electrons returning from CB to VB of the semiconductor, or electrons reacting with traps created due to defects in the material's crystals.

In comparison to pure ZnO, the gradual increase in photocurrent values for the ZnO:N-20 and ZnO:N-40 samples indicates that the charge separation process is favored by the presence of the dopant. This means that there is greater effectiveness in the separation of the e^-_{CB}/h^+_{VB} pair with consequent use of these charges in reduction and oxidation reactions that occur on the counter-electrode and surface of the semiconductor, respectively. Based on chronoamperometric curves, ZnO:N-60 film showed the shortest recombination time, justifying the reduction in its photocurrent value in the cyclic voltammetry curves presented in Fig. 5. In contrast, the ZnO:N-40 film displayed the longest time for charge recombination, i.e., the charges spend more time separated. This result corroborates the higher photocurrent value observed in the CV curves for the ZnO:N-40 sample, previously presented in Fig. 5b.

Under adequate irradiation, semiconductors are capable of generating electron–hole charges that react with water

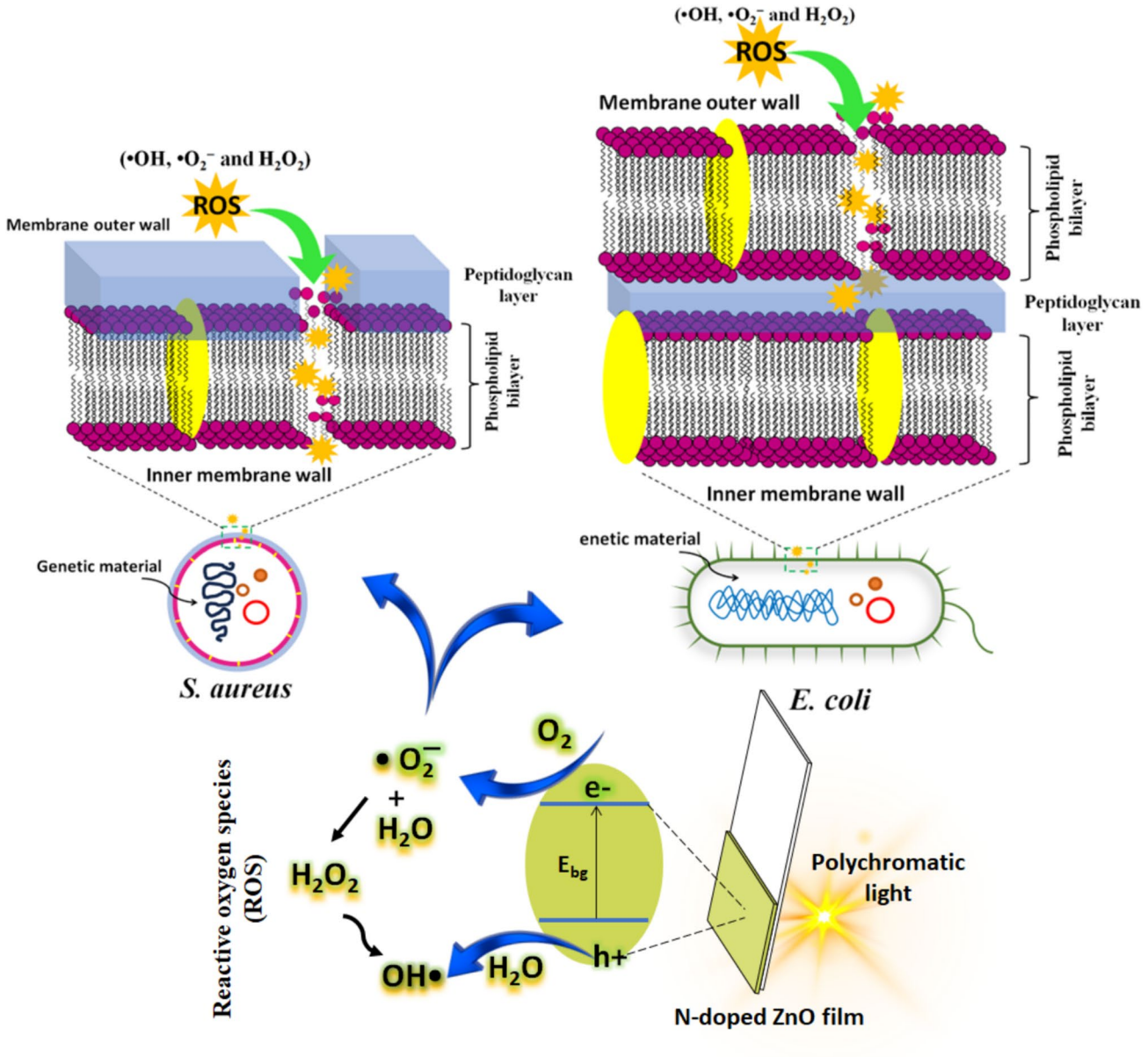

Fig. 10 Schematic representation of the formation of reactive oxygen species (ROS) on nitrogen doped zinc oxide electrode under polychromatic radiation and mechanism of action of ROS in the inactivation of *E. coli* and *S. aureus* bacteria

and oxygen molecules present in the electrolyte, forming reactive oxygen species (ROS) (Nosaka and Nosaka 2017). These ROS are formed with suitable positions of the VB and CB edge potentials of the semiconductor. The edge potentials can be estimated by photoelectrochemical measurements, considering the flat band potential (E_{fb}) of the material. Thus, linear sweep voltammograms (LSV) for ZnO and ZnO:N-40 electrodes calcined at 600 °C were recorded in light–dark conditions with a chopper at 10 s irradiation intervals. The LSV curves are shown in Fig. 7a, b. From the photocurrent curves, it was possible to estimate the E_{fb}, which can be approximated to the Fermi level potential by applying the Burter-Gärtner model, i.e., the variation of the square of the current (Costa et al. 2018). Thus, the Butler-Gartner model can be represented by Eq. 4:

$$I_{ph} = \alpha W_0 q \varphi_0 \sqrt{E - E_{fb}} \tag{4}$$

where (φ_0) is the irradiance, (α) is the absorption coefficient, (q) is the charge of the electron, (W_0) is the width of the depletion layer, and (E_{fb}) is the flat band potential. The E_{fb} values (Fig. 8) determined for the ZnO and ZnO:N-40 electrodes are − 0.083 and − 0.12 V, respectively.

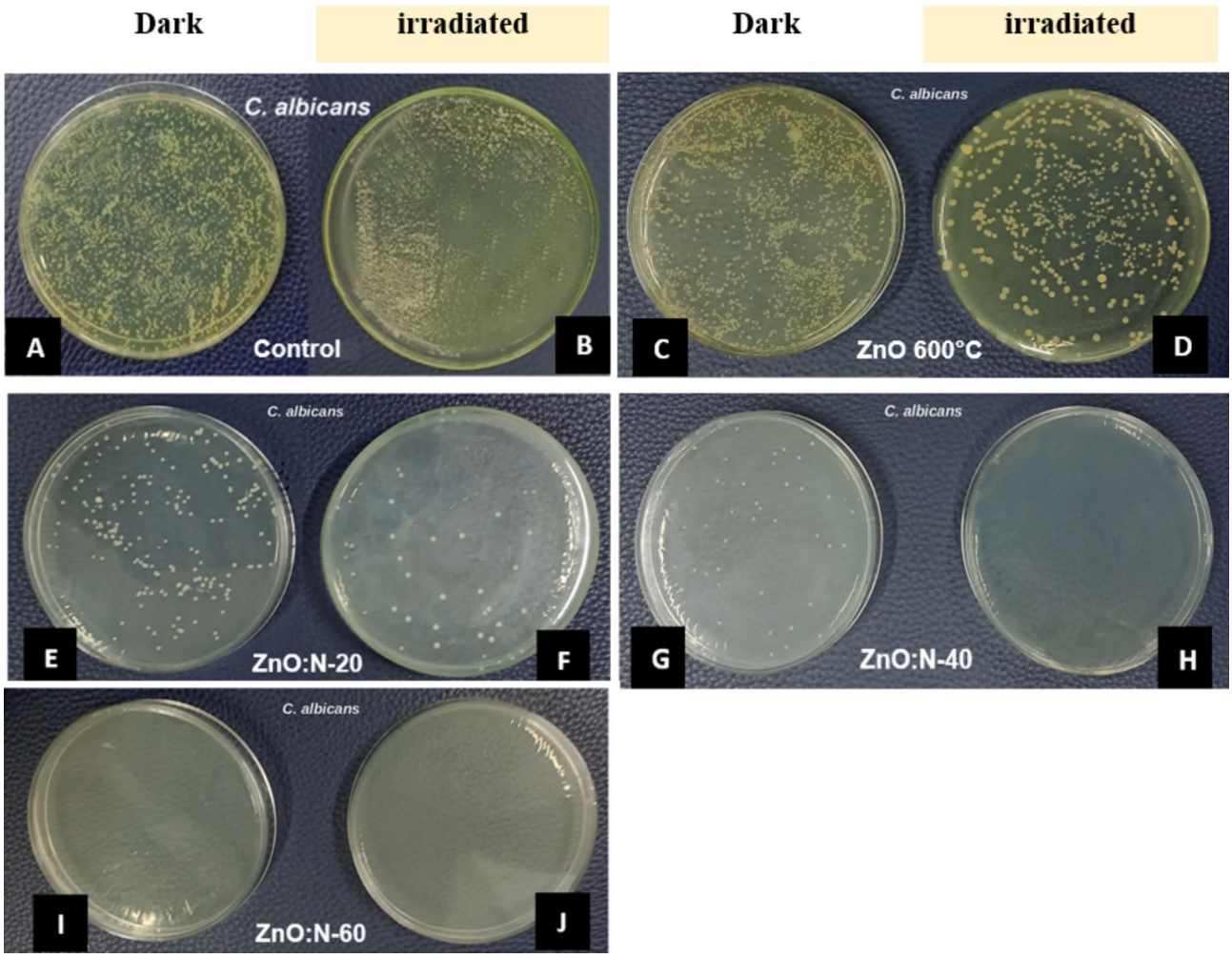

Fig. 11 Number of colonies grown after seeding in: **A**, **B** control of *C. albicans* growth in the dark and irradiated, **C**, **D** colonies of *C. albicans* with ZnO 600 °C in the dark and irradiated, **E**, **F** colonies of *C. albicans* with ZnO:N-20 in the dark and irradiated, **G**, **H** colonies of *C. albicans* with ZnO:N-40 in the dark and irradiated, **I**, **J** colonies of *C. albicans* with ZnO:N-60 in the dark and irradiated, respectively

Table 2 Antifungal activity of ZnO and ZnO:N films (20, 40, 60 cm^3 min^{-1}), under dark and irradiated conditions against *Candida albicans* (*C. albicans*)

Sample (condition)	Number of microorganism colonies per inactivation time (min)		
	C. albicans		
	10 min	20 min	30 min
Only action of light	*	*	*
ZnO (dark)	442	388	400
ZnO (irradiated)	286	286	120
ZnO:N-20 (dark)	115	92	41
ZnO:N-20 (irradiated)	37	24	17
ZnO:N-40 (dark)	57	27	11
ZnO:N-40 (irradiated)	–	–	–
ZnO:N-60 (dark)	6	2	–
ZnO:N-60 (irradiated)	3	–	–

In an n-type semiconductor, the Fermi level is located very close to the CB. Therefore, knowing E_{fb} can provide the position of one of the two bands, and so, the other can be estimated by knowing the E_{bg} of the semiconductor (Minella et al. 2015). Figure 8 shows the relative positions of the ZnO and ZnO:N-40 conduction and valence band edges, estimated on the vacuum energy scale relative to the Reversible Hydrogen Electrode (RHE) using Eqs. 1 and 2. Based on these E_{fb} and E_{bg} values, it was possible to establish the relative positions of the CB and VB on the RHE scale. Through this representation, it is possible to determine the oxidation potentials of each photoanode in photoelectrocatalytic processes. Band positions can reveal whether the reactions for generating ROS are thermodynamically favorable (Li et al. 2012).

Assessment of the antimicrobial activity of ZnO and ZnO:N films

The antibacterial activity of ZnO and ZnO:N samples (20, 40, 60 cm^3/min) was tested against Gram-positive bacteria (*S. aureus*) and Gram-negative bacteria (*E. coli)*. The tests were conducted in the absence of light (named of dark condition) or under polychromatic irradiation, using the colony counting method as an indicator of inhibition of microorganism growth. Figure 9 show photographs of antibacterial tests against *S. aureus* and *E. coli* for the control group conducted in 0.1 mol L^{-1} of Na_2SO_4 aqueous solution under dark or irradiated conditions, as well as for ZnO and ZnO:N films. The results obtained are presented in Table 1.

Only with the action of polychromatic irradiation was no inactivation of microorganisms observed. On the other hand, the presence of ZnO in the dark was able to reduce the growth of *S. aureus* bacteria colonies. The ZnO activity in the dark is very low or absent for *E. coli*. The asterisks (*) presented in Table 1 represent an uncountable number of microorganism colonies. When irradiated condition, the ZnO sample displayed inactivation activity for both types of bacteria. Under polychromatic light, ZnO has its electrons promoted from VB to CB, forming reactive oxygen species (ROS) such as hydroxyl radical (•OH), superoxide ($\bullet O_2^-$), and hydrogen peroxide (H_2O_2). Considering that under irradiation there is greater inactivation of microorganisms, we can state that ROS are mainly responsible for the death of *S. aureus* and *E. coli* bacteria. Thus, irradiation improves the activity of ZnO in removing bacteria. Figure 10 presents a proposed mechanism for ROS action and its action to inactivate both microorganisms.

The difference in the activity of ZnO in the inactivation of *S. aureus* and *E. coli* occurs due to the differences presented by the cell walls of these microorganisms. *S. aureus* is a Gram-positive (G+) bacterium, which has a cell membrane formed by an external peptidoglycan layer and an internal hydrophilic phospholipids bilayer (Kong et al. 2022; Ranjithkumar et al. 2021). On the other hand, *E. coli* is a Gram-negative (G−) bacterium with a cell wall composed of two phospholipids bilayer, interspersed with a thin layer of peptidoglycan (Rocha et al. 2023). The presence of these two phospholipid bilayer in G- bacteria make it more resistant to the action of ROS, formed on the irradiated ZnO electrodes. The higher photocurrent values for the N-doped ZnO (20 and 40%) electrodes are attributed to the greater separation of electron–hole charges and, consequently, the greater concentration of ROS formed on the electrodes. Also, as observed in Fig. 6, the ZnO:N-40 sample displayed the longest charge separation time and the highest photocurrent value. Thus, in agreement with the photoelectrochemical investigation, the photoelectrocatalytic studies showed that the ZnO:N-40 film was the most effective sample to inactivate G+ and G− bacteria. Another interesting result was that the doped samples showed greater biocidal activity for both bacteria, even in the non-irradiated condition.

The ZnO:N-60 sample showed bacterial activity in the dark. This result revealed that nitrogen strongly modified the initial bactericidal properties of ZnO. Previous studies published by Zheng and Wu (2008) evaluated the antibacterial activity of nitrogen doped ZnO nanocrystals on strains of *S. aureus* and *E. coli*. They suggested that the incorporation of nitrogen into the crystalline structure of ZnO improved the optical response of ZnO and increased antibacterial activity. Also, it was also seen that antibacterial activity against *S. aureus* and *E. coli* could be achieved even without irradiation. The authors attributed the bactericidal property of the material to oxygen vacancies and other defects in the ZnO crystals. As discussed here, in the XPS analyses, the presence of nitrogen as a dopant induced the formation of oxygen vacancies in ZnO. Furthermore, our photoelectrochemical characterization (Fig. 5b) indicate a reduction in photocurrent values and a higher rate of charge recombination for the ZnO:N-60 sample (Fig. 6). Also, our previous studies show that fast electron–hole pair recombination and lower photocurrent value indicate higher number of defects in the sample (Pitombeira et al. 2023; Luis et al. 2024). Therefore, the catalytic activity of the ZnO:N-60 sample in the dark can be understood as a result of defects in ZnO structure, caused by the introduction of a higher concentration of nitrogen as a dopant. Thus, ROS formed by both processes (action of light or defects) are capable of generating oxidative stress in the cell walls of bacteria, causing their death.

In addition to bactericidal activity, ZnO and N-doped ZnO samples were evaluated for their antifungal activity against *C. albicans*. Figure 11 illustrates photographs of the antifungal tests, and the results are presented in Table 2. As discussed early, the biocidal mechanism of ZnO and ZnO:N is strongly associated with the ROS generation. Thus, for C. albicans, ROS can affect its cellular components such as lipids, proteins and DNA (Djearamane et al. 1864). Pereira-Silva et al. (2019) investigated ZnO films and reported significant antifungal activity, demonstrating a strong capacity to inhibit cell growth. Table 2 shows that ZnO and ZnO:N exhibited strong antifungal activity against *C. albicans*, even under dark conditions. As previously discussed, the presence of the dopant increased the number of defects in the ZnO crystals, confirmed by the reduction in photocurrent values for the ZnO:Z-60 sample. These defects are also capable of generating ROS, which act in the process of inactivating fungi, even in absence of light. Also, the colony-forming units (CFUs) show a significant reduction under irradiation conditions, which confirms the increased generation of ROS by samples. CFUs indicate that increasing dopant concentration reduces fungal growth, which may be attributed the higher number of oxygen vacancies (Kumar et al. 2016).

Conclusion

The present study revealed that ZnO and ZnO:N films with hexagonal wurtzite structure were adequately prepared by the electrodeposition technique. The presence of the dopant altered the optical and electrical properties of ZnO. These results revealed that N doping showed that the dopant strongly influenced the photocurrent values recorded for the films. The E_{fb} value obtained for ZnO:N-40 shows that the VB and CB potentials are favorable in the formation of reactive oxygen species (ROS), which are capable of interacting with microorganisms. Thus, the efficiency of the pure and doped samples was evaluated in the inactivation of Gram-positive bacteria (*S. aureus*), Gram-negative bacteria (*E. coli*) and a species of yeast, unicellular fungus (*C. albicans*). In antimicrobial catalytic activity tests, all N-doped ZnO films showed efficacy in inhibiting *S. aureus*, *E. Coli* and *C. albicans* than pure ZnO. However, greater efficiency was observed for ZnO:N-40 sample under polychromatic irradiation. The formation of ROS is favored by the action of irradiation in photoelectrocatalysis. In addition, the favored oxygen vacancies in N-doped ZnO samples are also capable of forming ROS in the absence of light and therefore inactivating bacteria and fungi. Thus, this study on the biocidal activity of N-doped ZnO electrodes demonstrated for the first time the relationship between the photoelectrochemical characteristics and the biocidal activity of a semiconductor oxide for inactivation of microorganisms.

Supplementary Information The online version contains supplementary material available at https://doi.org/10.1007/s13762-025-06555-6.

Acknowledgements The authors would like to thank the research funding agencies FAPEPI, CAPES (88887.931740/2024-00) and CNPq (Process number 310720/2023-0) for scholarships granted to research participants and other financial support.

Funding The authors would like to thank the research funding agencies FAPEPI, CAPES (88887.931740/2024-00) and CNPq (Process number 310720/2023-0) for scholarships granted to research participants and other financial support.

Declarations

Conflict of interest The authors declare that they have no known competing financial interests or personal relationships that could have appeared to influence the work reported in this paper.

References

Ahmad T, Wani IA, Manzoor N, Ahmed J, Asiri AM (2013) Biosynthesis, structural characterization and antimicrobial activity of gold and silver nanoparticles. Colloids Surf B 107:227–234

Albertsson J, Abrahams SC, Kvick Å (1989) Atomic displacement, anharmonic thermal vibration, expansivity and pyroelectric coefficient thermal dependences in ZnO. Acta Crystallogr Sect B Struct Sci 45(1):34–40

Al-Gariaa AM, Elasala GS, Ismail EH, Khalil MMH, El-Sewify IM (2023) Photodegradation of antibacterial cefotaxime using Mn doped ZnO nanosphere. Inorg Chem Commun 158:111434

Amiri M, Etemadifar Z, Daneshkazemi A, Nateghi M (2017) Antimicrobial effect of copper oxide nanoparticles on some oral bacteria and *Candida* species. J Dent Biomater 4:347–352

Antonette LC, Shanthi J (2023) Degradation of Methylene Blue using methyltrimethoxysilane doped ZnO nanoparticles and inactivation of gram (+ve) and (-ve) bacteria. Results Chem 6:100998

Applerot G, Lipovsky A, Dror R, Perkas N, Nitzan Y, Lubart R, Gedanken A (2009) Enhanced antibacterial activity of nanocrystalline ZnO due to increased ros-mediated cell injury. Adv Funct Mater 19:842–852

Ardekani SR, Rouhaghdam AS, Nazari M (2018) n-doped ZnO-CuO nanocomposite prepared by one-step ultrasonic spray pyrolysis and its photocatalytic activity. Chem Phys Lett 705:19–22

Balestri A, Cardellini J, Berti D (2023) Gold and silver nanoparticles as tools to combat multidrug-resistant pathogens. Curr Opin Colloid Interface Sci 66:101710

Barbosa ML, Costa MJS, Lima AEB, Batista AM, Longo E, Cavalcante LS, Santos RS (2023) Anionic and cationic dyes removal by degradation via photoelectrocatalysis using a WO_3/$CuWO_4$ heterojunction film as a photoanode. Nano-Struct Nano-Objects 35:100993

Basu A, Misra AJ, Behera M, Behera SK, Nayak AK, Dhal NK, Tripathy SK (2021) Photocatalytic disinfection of extended-spectrum beta-lactamase producing *Escherichia coli* using alumina/ZnO heterostructures. J Environ Chem Eng 9(6):106334

Birkett M, Dover L, Cherian Lukose C, Wasy Zia A, Tambuwala MM, Serrano-Aroca Á (2022) Recent advances in metal-based antimicrobial coatings for high-touch surfaces. Int J Mol Sci 23(3):1162

Biron DS, Santos V, Bergmann CP (2021) Tubular ceramic membranes coated with ZnO and applied in the disinfection of water contaminated with *Staphylococcus aureus*. Ceram Int 47(19):27082–27090

Camargo LDO, Fontoura I, Veriato TS, Raniero L, Castilho ML (2023) Antibacterial activity of silver nanoparticles functionalized with amikacin applied against multidrug-resistant acinetobacter baumannii. Am J Infect Control 51(8):871–878

Carneiro RS, Canuto MR, Ribeiro LK, Ferreira DCL, Assunção AFC, Costa CACB, Uchôa VT (2022) Novel antibacterial efficacy of ZnO nanocrystals/ag nanoparticles loaded with extract of *Ximenia americana* L. (stem bark) for wound healing. S Afr J Bot 151:18–32

Catalano PN, Pezzoni M, Costa C, Soler GJDAA, Bellino MG, Desimone MF (2016) Optically transparent silver-loaded mesoporous thin film coating with long-lasting antibacterial activity. Micropor Mesopor Mater 236:158–166

Chen X, Wu Z, Liu D, Gao Z (2017) Preparation of Zno photocatalyst for the efficient and rapid photocatalytic degradation of azo dyes. Nanoscale Res Lett 12(1):143

Costa MJS, Costa GS, Lima AEB, Junior GEL, Longo E, Cavalcante LS, Santos RS (2018) Photocurrent response and progesterone degradation by employing WO_3 films modified with platinum and silver nanoparticles. ChemPlusChem 83(12):1153–1161

Costa D, Borges J, Mota MF, Rodrigues MS, Pereira-Silva P, Ferreira A, Vaz F (2019) Effect of microstructural changes in the biological behavior of magnetron sputtered ZnO thin films. J Vac Sci Technol A 37(1):011501

Dananjaya SHS, Kumar RS, Yang M, Nikapitiya C, Lee J, Zoysa M (2018) Synthesis, characterization of ZnO-chitosan nanocomposites and evaluation of its antifungal activity

against pathogenic *Candida albicans*. Int J Biol Macromol 108:1281–1288

Djearamane S, Xiu L-J, Wong L-S, Rajamani R, Bharathi D, Kayarohanam S, De Cruz AE, Tey L-H, Janakiraman AK, Aminuzzaman M et al (1864) Antifungal properties of zinc oxide nanoparticles on *Candida albicans*. Coatings 2022:12

Ejerhed L, Roshani L, Andersson AE (2020) Antimicrobial coating is associated with significantly lower aerobic colony counts in high-touch areas in an orthopedic ward environment. Ann Clin Microbiol Antimicrob 19(1):1–7

Escárcega-González CE, Garza-Cervantes JA, Vazquez-Rodríguez A, Montelongo-Peralta LZ, Treviño-Gonzalez MT, Díaz Barriga Castro E, Morones-Ramirez JR (2018) In vivo antimicrobial activity of silver nanoparticles produced via a green chemistry synthesis using *Acacia rigidula* as a reducing and capping agent. Int J Nanomed 13:2349–2363

Gu XQ, Zhu LP, Cao L, Ye ZZ, He HP, Chu PK (2011) Optical and electrical properties of ZnO:Al thin films synthesized by low-pressure pulsed laser deposition. Mater Sci Semicond Process 14(1):48–51

Gupta R, Eswar NK, Modak JM, Madras G (2016) Visible Light driven efficient n and Cu Co-doped ZnO for photo inactivation of *Escherichia coli*. RSC Adv 6(89):85675–85687

Hessien M (2022) Recent progress in zinc oxide nanomaterials and nanocomposites: from synthesis to applications. Ceram Int 48(16):22609–22628

Hopoğlu H, Aydinoğlu HS, Özer A, Tüzemen EŞ (2021) Investigation of nitrogen doped ZnO thin films: effects on their structural and optical properties. Opt Mater 122:111685

Kabir R, Saifullah MAK, Ahmed AZ, Masum SM, Molla MAI (2020) Synthesis of n-doped ZnO nanocomposites for sunlight photocatalytic degradation of textile dye pollutants. J Compos Sci 4(2):49

Khalid NR, Ishtiaq H, Ali F, Tahir MB, Naeem S, Ul-Hamid A, Ikram M, Iqbal T, Kamal MR, Alrobei H, Alzaid M, Dahshan A (2022) Synergistic effects of Bi and N doped on ZnO nanorods for efficient photocatalysis. Mater Chem Phys 289:126423

Khare T, Oak U, Shriram V, Verma SK, Kumar V (2019) Biologically synthesized nanomaterials and their antimicrobial potentials. Eng Nanometer Phytonanotechnol Chall Plant Sustain 87:263–289

Khatoon A, Hussain SF, Shahid SM, Kumar S, Khan SA, Shaikh OA, Nashwan AJ (2023) Emerging novel sequence types of *Staphylococcus aureus* in Pakistan. J Infect Public Health 17(1):51–59

Kong J, Zhang J, Shen M, Zhang S, Shen P, Ren C (2022) Preparation of manganese (ii) oxide doped zinc oxide nanocomposites with improved antibacterial activity via ros. Chem Phys Lett 806:140053

Kumar RS, Dananjaya SH, De Zoysa M, Yang M (2016) Enhanced antifungal activity of Ni-doped ZnO nanostructures under dark conditions. RSC Adv 6(110):108468–108476

Kumar P, Dev S, Kumar A, Thakur R, Dhar R (2021) Impact of indium doping on the anti-biofilm activity of ZnO thin films against Escherichia coli and *Staphylococcus aureus*. Superlatt Microstruct 150:106741

Li Y, Zhang W, Niu J, Chen Y (2012) Mechanism of photogenerated reactive oxygen species and correlation with the antibacterial properties of engineered metal-oxide nanoparticles. ACS Nano 6(6):5164–5173

Li W, Fang L, Ruan H, Qin G, Zhang P, Zhang H, Ye L, Kong C (2015) Oxygen vacancies induced ferromagnetism in Ag-N codoped ZnO thin films. Mater Lett 143:128–130

Luis JS, Eduardo SS, Costa MJS, Brandão-Lima L, Antunes RA, Ferreiras RO, Silva RMP, Santos RS (2024) S-doped ZnO photoelectrode modified with silver and platinum nanoparticles and their photocatalytic activity for progesterone degradation. J Mol Struct 1305:137764

Minella M, Maurino V, Minero C, Pelizzetti E (2015) Thin film nanocrystalline TiO_2 electrodes: dependence of flat band potential on pH and anion adsorption. Am J Nanosci Nanotechnol 15(5):3348–3358

Miri A, Mahdinejad N, Ebrahimy O, Khatami M, Sarani M (2019) Zinc oxide nanoparticles: biosynthesis, characterization, antifungal and cytotoxic activity. Mater Sci Eng C 104:109981

Mondal S, Ayon SA, Islam MS, Rana MS, Billah MM (2023) Morphological evaluation and boosted photocatalytic activity of N-doped ZnO nanoparticles prepared via Co-precipitation method. Heliyon 9:20948

Mu J, Shao C, Guo Z, Zhang Z, Zhang M, Zhang P, Liu Y (2011) High photocatalytic activity of ZnO−carbon nanofiber heteroarchitectures. ACS Appl Mater Interfaces 3(2):590–596

Nosaka Y, Nosaka AY (2017) Generation and detection of reactive oxygen species in photocatalysis. Chem Rev 17:11302–11336

Pasquet J, Chevalier Y, Pelletier J, Couval E, Bouvier D, Bolzinger MA (2014) The contribution of zinc ions to the antimicrobial activity of zinc oxide. Colloids Surf A 457:263–274

Pereira-Silva P, Costa-Barbosa A, Costa D, Rodrigues MS, Carvalho P, Borges J, Sampaio P (2019) Antifungal activity of ZnO thin films prepared by glancing angle deposition. Thin Solid Films 687:137461

Perkins CL, Lee SH, Li X, Asher SE, Coutts TJ (2005) Identification of nitrogen chemical states in N-doped ZnO via x-ray photoelectron spectroscopy. J Appl Phys 97:034907

Pitombeira DR, Costa MJ, Antunes RA, Ferreira RO, Silva RM, Santos RS (2023) Crystalline S-doped TiO_2 photoanodes from amorphous titanium oxysulfide (tioxsy) for photo-oxidation reactions. Opt Mater 142:114081

Qi K, Cheng B, Yu J, Ho W (2017) Review on the improvement of the photocatalytic and antibacterial activities of ZnO. J Alloys Compd 727:792–820

Ranjithkumar B, Kumar ER, Srinivas M, Ramalingam HB, Srinivas C, Magesh G, Chandarshekar B (2021) Evaluation of structural, surface morphological and thermal properties of Ag-doped ZnO nanoparticles for antimicrobial activities. Phys E 133:114801

Reis RY, Lima AE, Costa MJ, Cruz-Filho JF, Moura JP, Santos RS, Luz GE Jr (2020) Enhanced photoelectrocatalytic performance of ZnO films doped with N_2 by a facile electrochemical method. Surf Interfaces 21:100675

Resende AL, Costa AG, Lima AE, Costa MJ, Longo E, Cavalcante LS, Santos RS (2021) An investigation of photovoltaic devices based on p-type Cu_2O and n-type γ-WO_3 junction through an electrolyte solution containing a redox pair. Int J Energy Res 45(2):2797–2809

Rocha M, Araujo FP, Castro-lopes S, de Lima IS, Silva-Filho EC, Osajima JA, Peña-Garcia R (2023) Synthesis of Fe–Pr Co-doped ZnO nanoparticles: structural, optical and antibacterial properties. Ceram Inter 49(2):2282–2295

Sachivkina N, Podoprigora I, Bokov D (2021) Morphological characteristics of *Candida albicans*, *Candida krusei*, *Candida guilliermondii*, and *Candida glabrata* biofilms, and response to farnesol. Vet World 14(6):1608

Sinornate W, Mimura H, Pecharapa W (2022) Structural, optical and electrical properties of Sb-doped ZnO/ZnO homojunction thin film structures prepared by sol-gel based coating process under nitrogen annealing atmosphere. Optic 265:169445

Tang J, Wei F, Zhao L, Yang L, Li J, Sun Z, Liu B (2023) Superior antibacterial properties of copper-doped titanium oxide films prepared by micro-arc oxidation. Ceram Int 50:1370–1378

Tang JF, Yang YL, Chen LC, Kang CF, Hsu CL (2024) Gas-sensing properties of p-type of nitrogen-doped ZnO nanorods prepared by deep cryogenic treatment. Appl Surf Sci 658:159871

Tiron V, Velicu IL, Stanescu D, Magnan H, Sirghi L (2017) High visible light photocatalytic activity of nitrogen-doped ZnO thin films deposited by hipims. Surf Coat Technol 324:594–600

Wu C, Zhang YC, Huang Q (2014) Solvothermal synthesis of n-doped ZnO microcrystals from commercial ZnO powder with visible light-driven photocatalytic activity. Mater Lett 119:104–106

Yurtsever MÇ, Cömertpay A, Iyigundogdu Z, Yurtsever HA (2024) Room temperature biosynthesis of ZnO nanoparticles using avocado seed extract with antimicrobial and anticancer properties. Int J Environ Sci Technol 21:8025–8038

Zhang G, Zhang N, Xu J, Yang T, Yin H, Cai Y (2023a) Efficacy and safety of vancomycin for the treatment of *Staphylococcus aureus* bacteremia: a systematic review and meta-analysis. Int J Antimicrob Agents 62:106946

Zhang X, Zhou L, Tu X, Hu F (2023b) Hydrothermal synthesis of ZnO crystals: diverse morphologies and characterization of the photocatalytic properties. Polyhedron 246:116668

Zheng M, Wu J (2008) One-step synthesis of nitrogen-doped ZnO nanocrystallites and their properties. Appl Surf Sci 255(11):5656–5661